

Quadric hypersurface intersection for manifold learning in feature space

Fedor Pavutnitskiy^{*1} Sergei O. Ivanov^{*2} Evgeny Abramov^{*2} Viacheslav Borovitskiy^{*2,3} Artem Klochkov^{*2}
Viktor Vialov^{*2} Anatolii Zaikovskii^{*2} Aleksandr Petiushko⁴

Abstract

The knowledge that data lies close to a particular submanifold of the ambient Euclidean space may be useful in a number of ways. For instance, one may want to automatically mark any point far away from the submanifold as an outlier, or to use its geodesic distance to measure similarity between points. Classical problems for manifold learning are often posed in a very high dimension, e.g. for spaces of images or spaces of representations of words. Today, with deep representation learning on the rise in areas such as computer vision and natural language processing, many problems of this kind may be transformed into problems of moderately high dimension, typically of the order of hundreds. Motivated by this, we propose a manifold learning technique suitable for moderately high dimension and large datasets. The manifold is learned from the training data in the form of an intersection of quadric hypersurfaces—simple but expressive objects. At test time, this manifold can be used to introduce an outlier score for arbitrary new points and to improve a given similarity metric by incorporating learned geometric structure into it.

1. Introduction

Manifold learning techniques are applied to data visualization and interpretation (Patwari et al., 2005), to feature learning (Lunga et al., 2013), and to anomaly detection and similarity learning (Du and Zhang, 2014). The main idea behind the latter group of applications is that if we know the underlying manifold we can use its geodesic distance to define similarity and, at the same time, we can use the projection distance from a point in the ambient space to the manifold as an outlier score.

^{*}Equal contribution ¹HSE University ²St. Petersburg State University ³St. Petersburg Department of Steklov Mathematical Institute of Russian Academy of Sciences ⁴Moscow State University. Correspondence to: Fedor Pavutnitskiy <fedor.pavutnitskiy@gmail.com>.

One particularly interesting new area of research for manifold learning is motivated by the recent advances in deep representation learning, which is strikingly effective in many areas including computer vision (Deng et al., 2019) and natural language processing (Devlin et al., 2018). In a wide range of industrial scenarios where deep representation learning is used as a part of a larger pipeline, a feature space level outlier detector may help tackle the problem of out-of-distribution input data at test time, which, in its turn, may appear due to undertraining, faulty preprocessing or even a deliberate attack. Manifold learning may be used to build such a detector. Moreover, in other problems where the deep representation model is used to compare the similarity of different inputs, e.g. in face recognition, manifold learning may be used to either find a natural metric in feature space or to modify and improve an existing one.

Motivated by the problem of feature space level outlier detection and similarity metric improvement, we propose a manifold learning technique where the manifold is learned in form of an intersection of quadric hypersurfaces—the zero-sets of quadratic polynomials. Similarly to the classical principal component analysis (PCA), our technique yields an explicit manifold as a subset of the ambient Euclidean space. Leveraging this, it is possible to compute the approximate projection distance from an arbitrary point to this manifold at test time, which enables us to define an outlier score and to improve a given similarity metric by penalizing outliers.

The proposed quadric hypersurface intersection model is much more expressive than the linear one used in PCA, which is the intersection of hyperplanes.¹ At the same time, the number of parameters that define this model grows quadratically with the dimension, thus making it suitable for moderately high-dimensional spaces. Fitting a quadric hypersurface intersection to data is an optimization problem, which we pose so as to facilitate robustness and to achieve equivariance with respect to the action of the Euclidean group meaning e.g. that the optimal fit for a rotated point cloud is the rotation of the optimal fit for the initial point cloud. We solve the optimization problem using a stochastic gradient descent based algorithm thus allowing the tech-

¹An additional justification for the expressiveness of the model can be found in Mumford (2010, Theorem 1).

nique to scale well with the size of the training dataset.

The need for a new technique comes from the fact that classical non-linear manifold learning algorithms are usually *not* designed for outlier-detection use cases, where one has a point cloud for training and then needs to make judgements about new points that arrive one by one at test time. For instance, Isomap (Tenenbaum et al., 2000), LLE (Roweis and Saul, 2000), Laplacian eigenmaps (Belkin and Niyogi, 2001), t-SNE (Maaten and Hinton, 2008) and UMAP (McInnes et al., 2018) are methods of this kind that do not easily support the computation of projective distances for a new test point. Other methods, most notably PCA and Kernel PCA (Schölkopf et al., 1998) support the necessary computations but can fail to be expressive enough or scale poorly with either the dimension of the ambient space, or cardinality of the training dataset, or both.

To showcase the potential of the proposed technique, we consider its application to an image classification and outlier detection problem.

2. Manifold learning

Manifold learning, as a term, refers to a diverse collection of techniques motivated by the *manifold hypothesis* (Fefferman et al., 2016), the statement that natural datasets (e.g. images of pets) lie in the vicinity of a relatively low-dimensional manifold embedded in a higher-dimensional ambient Euclidean space. Manifold learning is commonly considered synonymous to *nonlinear dimensionality reduction* (Lee and Verleysen, 2007), though the latter more often refers to data-visualization methods.

There exists a large set of manifold learning techniques, many of them are considered by Ma and Fu (2011). Most of these techniques can be thought of as black boxes which take a point cloud in a high-dimensional Euclidean space and which map every point of the cloud into a point in a low-dimensional Euclidean space. For example, multidimensional scaling algorithms seek the mapping so as to preserve pairwise distances as well as possible, while PCA, when viewed through the appropriate lens, tries to preserve as much of the data’s variation as possible.

Another natural but less-often studied class of manifold learning techniques tries to characterize the manifold in the vicinity of which the point cloud lies as a submanifold of an ambient Euclidean space. We highlight that this shift in formulation allows one to ask additional questions, such as how far an arbitrary point in the ambient space is from the manifold—a key question for the outlier detection applications. We proceed to discuss this formulation further.

2.1. Characterizing manifolds

We begin by recalling and highlighting a key property of principal component analysis, namely that it characterizes the manifold it finds as a submanifold of the ambient Euclidean space. Given a centered point cloud $p_1, \dots, p_n \in \mathbb{R}^d$, PCA finds orthonormal vectors $v_1, \dots, v_d \in \mathbb{R}^d$ such that

$$V_k = \{x \in \mathbb{R}^d \mid x = \alpha_1 v_1 + \dots + \alpha_k v_k\} \quad (1)$$

is the k -dimensional linear subspace (thus a submanifold) of the ambient Euclidean space \mathbb{R}^d that optimally fits the point cloud in a suitable sense. With this definition, it is possible to compute the distance from any point $p \in \mathbb{R}^d$ to the closest point of V_k :

$$d(p, V_k) = \left\| p - \sum_{j=1}^k \langle p, v_j \rangle v_j \right\| = \left(\sum_{j=k+1}^d \langle p, v_j \rangle^2 \right)^{1/2}, \quad (2)$$

where $\|\cdot\|$ and $\langle \cdot, \cdot \rangle$ are standard Euclidean norm and inner product, respectively. In this sense, PCA explicitly characterizes the manifold through (1).

PCA’s way of characterizing a manifold is very convenient but relies on the fact that elements of a linear subspace can be represented as linear combinations of a finite collection of basis vectors, which does not directly extend to non-linear spaces. However, one can modify this point of view, to make it more amenable to the non-linear setting by considering the linear subspace that PCA finds as the zero set of some vector-valued linear mapping. Define $F_k : \mathbb{R}^d \rightarrow \mathbb{R}^{d-k}$ by $F_k(x) = (\langle x, v_{k+1} \rangle, \dots, \langle x, v_d \rangle)$ and denote, for arbitrary F , its zero set

$$Z(F) = \{x \in \mathbb{R}^d \mid F(x) = 0\}. \quad (3)$$

Then we have $V_k = Z(F_k)$. This is an instance of a very general way of representing a submanifold, as a zero set of some smooth function: rather than viewing the manifold as the span of a set of basis vectors, we can view the manifold as a solution to the system of equations $Z(F) = 0$.

By the preimage theorem (Milnor and Weaver, 1997, §2, Lemma 1), under mild technical assumptions on F , we have that $Z(F)$ is indeed a manifold. Moreover, any submanifold $\mathcal{M} \subseteq \mathbb{R}^d$ can be represented this way, take for instance $F(x) = d(x, \mathcal{M}) = \inf_{x' \in \mathcal{M}} d(x, x')$, the distance from x to the manifold \mathcal{M} .

In the following, we will rely on representing a manifold as a zero set of a function, thus shifting the problem of finding a manifold to the problem of finding a suitable function.

Note that this representation is much more expressive (though less explicit) than representing a manifold as an image of \mathbb{R}^k under some function $G : \mathbb{R}^k \rightarrow \mathbb{R}^d$ as for

the mapping $G(\alpha_1, \dots, \alpha_k) = \alpha_1 v_1 + \dots + \alpha_k v_k$ in PCA. Although this method is widely used, for example in autoencoder neural networks, it can only represent manifolds that can be covered by a single chart: this prevents the accurate representation of, for instance, the simple sphere or torus.

3. Intersections of quadric hypersurfaces

As noted in the previous section, the k -dimensional submanifold of \mathbb{R}^d that PCA finds from a point cloud $p_1, \dots, p_n \in \mathbb{R}^d$ is a zero set $Z(F)$ of some linear function $F : \mathbb{R}^d \rightarrow \mathbb{R}^{d-k}$. If we look a little bit deeper at how this manifold is defined, we can see that F solves the optimization problem

$$\sum_{j=1}^n d(p_j, Z(F))^2 \rightarrow \min. \quad (4)$$

Recall that $F = (f_1, \dots, f_{d-k})$ where $f_j(x) = \langle x, u_j \rangle$ are linear polynomials with coefficients $u_j \in \mathbb{R}^d$ such that vectors u_1, \dots, u_{d-k} are orthonormal. It means that (4) has to be optimized over $d - k$ vectors u_j of dimension d under the constraint that they should form an orthonormal system. Expanding the distance in (4) through (2), we get a simple convex optimization problem which can either be solved exactly by computing the singular value decomposition (SVD) of some $d \times n$ matrix, or approximately through gradient-based optimization.

We propose to extend this by considering quadratic polynomials f_j instead of the linear ones, as components of function F .

The zero set of a quadratic polynomial (polynomial of degree 2) is called a *quadric hypersurface* or simply a *quadric*. We consider linear polynomials and constants to be special cases of quadratic polynomials and similarly refer to their zero sets as quadrics. The word *hypersurface* is justified by the fact that in the non-degenerate case $Z(f_j)$ are $(d - 1)$ -dimensional manifolds.²

Moreover, the zero set $Z(F)$, which coincides with the intersection

$$Z(F) = Z(f_1) \cap \dots \cap Z(f_{d-k}), \quad (5)$$

is, in this non-degenerate case, a k -dimensional manifold, since each of $d - k$ quadrics eliminates one dimension of the d -dimensional ambient space.

Quadrics in \mathbb{R}^2 are conic sections: ellipses, hyperbolas and parabolas. However already in \mathbb{R}^3 quadrics and their intersections may be much more nontrivial. This is illustrated

²A quadric hypersurface is non-degenerate if the Hessian matrix of the homogenization $f^{\text{hom}}(x_1, \dots, x_{d+1}) = x_{d+1}^2 f(x_1/x_{d+1}, \dots, x_d/x_{d+1})$ of the corresponding polynomial f is non-singular. In this case the quadric is a smooth algebraic variety and thus a manifold of dimension $d - 1$ (Harris, 2013, Example 3.3).

on Figure 1. We refer the reader to the paper of Beale et al. (2016) and to the references therein for a brief review of the previous work on the topic of fitting quadrics in low dimension, while proceeding to present an algorithm suitable for high dimension and large datasets.

3.1. Fitting a quadric intersection to a point cloud

We start with the optimization problem (4), which, at least in theory, is as applicable for intersections of quadrics as it is to linear subspaces (intersections of linear hypersurfaces). Any quadratic polynomial in \mathbb{R}^d can be written as

$$f(x) = \sum_{i \leq j} \alpha_{i,j} x_i x_j + \sum_i \alpha'_i x_i + \alpha'', \quad (6)$$

where $\alpha_{i,j}, \alpha'_i, \alpha'' \in \mathbb{R}$. We denote the vector of its coefficients by $v(f) = (\alpha_{1,1}, \dots, \alpha_{d,d}, \alpha'_1, \dots, \alpha'_d, \alpha'')^T \in \mathbb{R}^D$, where $D = (d^2 + 3d)/2 + 1$ is the number of monomials of degree ≤ 2 in d variables. Thus the intersection of quadrics $Z(f_1), \dots, Z(f_m)$ is determined by m vectors $v(f_1), \dots, v(f_m)$, similarly to how a linear subspace is determined by the basis vectors in PCA.

The intersection of quadrics $Z(F)$ does not change if we make a replacement $f_i \mapsto a f_i$ for $a \neq 0$ or $f_i \mapsto f_i + a f_j$ for any $a \in \mathbb{R}$ and $i \neq j$, which is quite clear from viewing the $Z(F)$ as the solution set of a system of equations. Moreover, the problem (4) per se has $F(x) \equiv 0$ for a trivial solution that corresponds to the whole $Z(F) = \mathbb{R}^d$. To handle this, we need to introduce some constraints to the optimization problem. We therefore look for an *orthonormal* collection of quadratic polynomials with respect to some inner product, the most simple of which is the standard inner product of vectors $v(f_1), \dots, v(f_m)$.

It turns out though that (4) is very hard to solve for quadrics: computing even a single $d(p_j, Z(f_k))$ is a (computationally) hard problem because projecting a point onto a quadric is nontrivial. A number of approximations have therefore been proposed (Taubin, 1991; Taubin, 1993) such as $d_{\text{alg}}(p_j, Z(f_k)) := |f_k(p_j)|$, called the *algebraic distance*. Approximating $d(p_j, Z(F)) \approx (\sum_{k=1}^m |f_k(p_j)|^2)^{1/2}$, gives the optimization problem

$$\sum_{j=1}^n \sum_{k=1}^m |f_k(p_j)|^2 \frac{\|v(f_k)\|=1}{v(f_k) \perp v(f_i)} \rightarrow \min. \quad (7)$$

To fit a quadric intersection, we can solve this problem with the (stochastic) gradient descent. We will further improve this technique further in the sequel.

Connection to PCA Consider a feature map $\varphi : \mathbb{R}^d \rightarrow \mathbb{R}^D$ that is given by

$$\varphi(p) = (\underbrace{\dots, p_i p_j, \dots}_{\text{pairwise products}}, \underbrace{p_1, \dots, p_d}_{\text{coordinates}}, \underbrace{1}_{\text{constant}})^T. \quad (8)$$

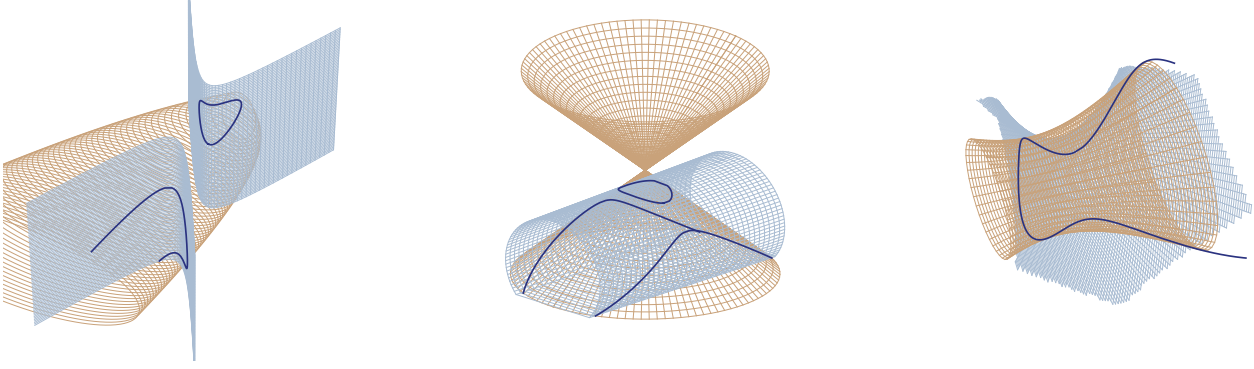


Figure 1: Examples of quadrics and their intersections in \mathbb{R}^3 . Two quadric surfaces are depicted by two meshes, each with its own color. The dark blue line portrays their intersection. From left to right: the intersection of an elliptic paraboloid with a hyperbolic cylinder; the intersection of an elliptic cone with an elliptic cylinder; the intersection of a hyperbolic hyperboloid and a hyperbolic paraboloid.

For a quadratic polynomial f we have $f(p) = \varphi(p)^\top \cdot v(f)$. A simple computation (see Appendix A for details) yields

$$\sum_{j=1}^n \sum_{k=1}^m |f_k(p_j)|^2 = \sum_{j=1}^n d(\varphi(p_j), \mathcal{V}_m^\perp)^2, \quad (9)$$

where \mathcal{V}_m is a linear subspace of \mathbb{R}^D spanned by vectors $v(f_1), \dots, v(f_m)$ and \mathcal{V}_m^\perp is its orthogonal complement. It follows that the optimization problem is equivalent to minimization of $\sum_{j=1}^n d(\varphi(p_j), \mathcal{V}_m^\perp)^2$, the same problem that PCA solves. This means that the technique presented above is equivalent to applying PCA in a feature space defined by (8), when viewed from a different angle.

A slight modification of the feature map (8) that is given by $\tilde{\varphi}(p) = (\dots, p_i p_j, \dots, \sqrt{2} p_1, \dots, \sqrt{2} p_d, 1)^\top$ corresponds to the polynomial kernel $k(x, y) = (\langle x, y \rangle + 1)^2$ of degree 2 in the sense that $k(x, y) = \langle \tilde{\varphi}(x), \tilde{\varphi}(y) \rangle$. This shows that the optimization problem is closely connected with kernel PCA with a polynomial kernel.³

This suggests an alternative way of solving the optimization problem (7)—by computing the SVD of a $D \times D$ matrix, although it is usually impractical since D depends quadratically on d and the computational complexity of SVD is of order $O(D^3) = O(d^6)$.

Discussion The technique presented above has some downsides. First, the algebraic distance is a rather poor approximation of the geometric distance. In practice, this may result in artifacts and unstable behavior of gradient-based optimization. Second, the technique’s deep connection to PCA suggests that it may be very sensitive to outliers, similar to

how PCA is (Candès et al., 2011). Finally, the optimization problem (7) does not reflect well the geometric structure of the manifold learning problem as it is non-equivariant in the following sense. If f_1, \dots, f_m is an orthonormal collection of quadratic polynomials and $\theta : \mathbb{R}^d \rightarrow \mathbb{R}^d$ is an isometry, then the collection $f_1 \circ \theta, \dots, f_m \circ \theta$ can fail to solve the optimization problem (7) for the point cloud transformed by θ (see Appendix A). Below we address these downsides and present a more refined technique for fitting an intersection of quadrics to a point cloud.

3.2. An improved loss function

In the preceding section, the intractability of computing the geometric distance $d(p, Z(f))$ for quadrics motivated the need for approximations. As an initial candidate, we previously considered the simplest approximation, namely the algebraic distance $d_{\text{alg}}(p, Z(f))$, which unfortunately led us to a number of difficulties. We therefore now consider alternatives. In Taubin (1993) a notion $d_k(p, Z(f))$ of *approximation distance of order k* is defined, building upon the idea of k -th order Taylor approximation. This distance coincides with the only non-negative root of a certain polynomial $c_0 + c_1 t + \dots + c_k t^k$ of degree k , whose coefficients depend on partial derivatives of f in p —full details are given in Appendix A. One particularly popular approximation of a distance is the *distance of order 1* given by $d_1(p, Z(f)) = |f(p)| / \|\nabla f(p)\|$. For a quadratic polynomial f , the k -distance coincides with the 2-distance for $k \geq 2$. Moreover, there is a simple explicit formula for the 2-distance, namely, it is a root of a quadratic polynomial with explicit coefficients depending on p and f :

$$d_2(p, Z(f)) = \frac{\sqrt{h^2 + |f(p)| \|f\|_{HS}} - h}{\|f\|_{HS}}, \quad (10)$$

³The feature map (8) is also similar to the Veronese map of degree 2 used in Generalized PCA (Vidal et al., 2005, §3.1). The difference is we consider not only quadratics, but all monomials of degree ≤ 2 .

where $h = \|\nabla f(p)\|/2$, and $\|f\|_{HS}$ is a certain Hilbert-Schmidt norm defined in (14) below

The distance of order 2 gives a better approximation of the geometric distance in a number of ways. Firstly, as the geometric distance $d(p, Z(f)) = \inf_{x \in Z(f)} \|p - x\|$, it is equivariant with respect to the action of the Euclidean group. More precisely, for isometries $\theta : \mathbb{R}^d \rightarrow \mathbb{R}^d$ we have

$$d_2(\theta(p), Z(f \circ \theta)) = d_2(p, Z(f)). \quad (11)$$

The proof of this fact can be found in Appendix A. Secondly, it is majorized by the geometric distance

$$d_2(p, Z(f)) \leq d(p, Z(f)), \quad (12)$$

(see Taubin (1991, §6)) while d_{alg} and d_1 are not (the latter may even be infinite). This limits the contribution of the outliers to the optimization objective and thus facilitates robustness. Finally, this distance is simple to compute. Hence, for quadrics, the distance of order 2 constitutes a great candidate for the approximation of the geometric distance.

Recall that in order to define a new optimization objective, we have to approximate $d(p, Z(F))$ for $F = (f_1, \dots, f_m)$, not just $d(p, Z(f_k))$. In Section 3.1, we used the l^2 -based term $(\sum_{k=1}^m |d_{\text{alg}}(p, Z(f_k))|^2)^{1/2}$ as a proxy for $d(p, Z(f))$. Here, we suggest to use the l^1 -based term $\sum_{k=1}^m |d_2(p, Z(f_k))|$ to approximate the geometric distance, based on the consideration that l^1 -loss is usually more robust to outliers than the squared l^2 -loss, simply because $|x|$ is smaller than $|x|^2$ for large x . This change also leads to equivariance of the objective, as equivariance of each term of the sum implies equivariance of the whole sum.

3.3. Improved constraints

By replacing d_{alg} with d_2 , we have made the optimization objective equivariant with respect to the action of the Euclidean group. Unfortunately, since the coefficient-wise inner product for quadratic polynomials is not equivariant, the constrained optimization problem still exhibits geometrically unnatural behavior. To resolve this, we suggest an alternative inner product for quadrics such that the constraint of orthonormality with respect to this inner product makes the whole optimization problem equivariant.

Any quadratic polynomial f can be represented in form

$$f(x) = x^\top A x + b x + c, \quad (13)$$

where A is a symmetric $d \times d$ matrix, b is a row vector and $c \in \mathbb{R}$. If $f(x) = \sum_{i \leq j} \alpha_{i,j} x_i x_j + \sum_i \alpha'_i x_i + \alpha''$, as in (6) then $A_{i,i} = \alpha_{i,i}$ and $A_{i,j} = A_{j,i} = \alpha_{i,j}/2$ for $i < j$.

If f and g are quadratic polynomials with corresponding symmetric matrices A and B , we define their Hilbert-Schmidt (degenerate) inner product as the Hilbert-Schmidt

inner product of their matrices

$$\langle f, g \rangle_{HS} = \sum_{i,j} A_{ij} B_{ij}, \quad \|f\|_{HS} = \sqrt{\langle f, f \rangle_{HS}} \quad (14)$$

This inner product is degenerate in the sense that the corresponding norm $\|f\|_{HS}$ is actually only a seminorm, i.e. $\|f\|_{HS} = 0$ does not imply $f = 0$, this is because it vanishes on polynomials of degree ≤ 1 . A collection of quadratic polynomials f_1, \dots, f_m is called HS-orthonormal if it is orthonormal with respect to the Hilbert-Schmidt inner product. In particular, an HS-orthonormal collection of quadratic polynomials consists only of polynomials of degree 2.⁴

It is easy to check (see Appendix A for details) that this inner product is equivariant with respect to the action of the Euclidean group. Specifically, for any isometry $\theta : \mathbb{R}^d \rightarrow \mathbb{R}^d$ the following holds:

$$\langle f, g \rangle_{HS} = \langle f \circ \theta, g \circ \theta \rangle_{HS}. \quad (15)$$

If we define the weighted vector of quadratic coefficients

$$\tilde{v}(f) = (\alpha_{1,1}, \alpha_{1,2}/\sqrt{2}, \dots, \alpha_{d-1,d}/\sqrt{2}, \alpha_{d,d})^\top, \quad (16)$$

where all coefficients that correspond to the non-diagonal entries of A are divided by $\sqrt{2}$, then, we have $\langle f, g \rangle_{HS} = \langle \tilde{v}(f), \tilde{v}(g) \rangle$, with the regular Euclidean inner product on the right-hand-side.

There is a number of ways to enforce orthonormality of $\tilde{v}(f_1), \dots, \tilde{v}(f_m)$. The problem is well-studied in the context of orthogonality of filters inside the convolution layers of neural networks (cf. (Bansal et al., 2018)). We propose to use the soft orthogonality regularization term $\|X(F)^T X(F) - I\|_{HS}^2$, where

$$X(F) = (\tilde{v}(f_1), \dots, \tilde{v}(f_m)) \quad (17)$$

is a $d(d+1)/2 \times m$ -matrix, whose columns are $\tilde{v}(f_i)$.

3.4. An outlier-robust and equivariant algorithm

Assume that we have a cloud of points $p_1, \dots, p_n \in \mathbb{R}^d$ and we want to find m quadratic polynomials f_1, \dots, f_m so that this cloud lies geometrically close to the intersection of quadrics $Z(f_1) \cap \dots \cap Z(f_m)$. Formally, we pose the optimization problem as follows

$$\sum_{j=1}^n \sum_{k=1}^m |d_2(p_j, Z(f_k))| \xrightarrow[\langle f_k, f_l \rangle_{HS}=0]{\|f_k\|_{HS}=1} \min, \quad (18)$$

⁴Note that such a collection can still be used to represent a linear subspace, simply because a linear equation of form $f(x) = 0$ may be transformed into a quadratic equation $f(x)^2 = 0$ with the same solution.

where each of m quadrics f_k is represented by the D -dimensional vector of its coefficients. Since both the optimization objective and the constraints are equivariant, the whole optimization problem is equivariant: if quadrics f_1, \dots, f_m solve the optimization problem above, then for any isometry $\theta : \mathbb{R}^d \rightarrow \mathbb{R}^d$ the collection $f_1 \circ \theta, \dots, f_m \circ \theta$ solves the same optimization problem for the transformed point cloud $\theta(p_1), \dots, \theta(p_n)$. Moreover, as discussed in Section 3.2, the optimization objective is designed to be more robust than the simpler one from Section 3.1. The robustness claim is additionally supported by the results of a toy experiment presented in Section 4.1.

In practice, we employ a soft constraint incorporated into the loss that is given by the Lagrangian

$$\sum_{j=1}^n \sum_{k=1}^m |d_2(p_j, Z(f_k))| + \lambda \|X(F)^T X(F) - I\|_{HS}^2, \quad (19)$$

where $X(F)$ is as above and λ is a hyperparameter. We solve this via the stochastic gradient descent over the $D \times m$ -dimensional set of quadric coefficients.

3.5. Out-of-distribution detection

In the real world applications the deep representation learning models are sometimes held back by a number of problems. A particularly important one is the out-of-distribution input data at test time: a model deployed as part of a larger pipeline may be subject to a malfunctioning preprocessing or, say, a deliberate attack. An out-of-distribution detector at the level of the model’s feature space may serve as an additional line of defense in such scenarios.

Assuming a moderately high (order of hundreds) dimensional feature space, we may fit an intersection of quadrics to the feature embeddings of the training data, as described in the previous section. The assumption that the embeddings lie close to the found manifold suggests the distance of a point to manifold as a natural outlier score.

Since it is computationally difficult to evaluate this distance exactly, we suggest using the same approximation that was utilized for training. Specifically, we define the outlier score $o(p)$ of an arbitrary point p in the embedding space by

$$o(p) = \frac{1}{m} \sum_{k=1}^m d_2(p, Z(f_k)), \quad (20)$$

where f_1, \dots, f_m are the quadratic polynomials that define the found manifold. This average, while easy to compute, may serve as an effective out-of-distribution score. In Section 4 we evaluate the performance of the out-of-distribution detector built upon this construction.⁵

⁵Note that this score may alternatively be viewed as the combined score of the ensemble of simple out-of-distribution detectors (individual quadrics).

3.6. Similarity metric robustification

Typically, classifiers built on top of deep representation learning models are based upon some simple notion of similarity between embeddings, defined usually through Euclidean or cosine distance (Deng et al., 2019). By fitting a quadric intersection manifold to the set of embeddings of the training data, we obtain additional geometric structure that can be incorporated into the similarity metric.

The most natural way to incorporate the geometric structure is to use the geodesic distance of the manifold as the new similarity function. Unfortunately though, computing the geodesic distance between a pair of points on the intersection of quadrics manifold is a difficult problem rendering such an approach impractical.

On the other hand, a different approach can be used to improve a given similarity metric (e.g. Euclidean) using the found geometric structure. Namely, by incorporating the information of the outlierness of points into the metric, we can make classification more robust. For instance, we can consider the following modifications of a given similarity function s .

- Soft penalty for the points with high outlier score:

$$s_s(x, y) = s(x, y) - \alpha \max(o(x), o(y)). \quad (21)$$

Here $o(\cdot)$ is as above and $\alpha \in \mathbb{R}_+$ is a hyperparameter for tuning the relative effect of the outlierness as compared to the original similarity function.

- Declaring the outliers dissimilar to anything:

$$s_h(x, y) = \begin{cases} s(x, y), & \max(o(x), o(y)) < t, \\ 0, & \max(o(x), o(y)) \geq t, \end{cases} \quad (22)$$

where t is a threshold hyperparameter.

The hyperparameters may be chosen by analyzing the data or fit using an additional calibration dataset.

4. Experiments

4.1. Toy example

To illustrate the proposed technique and compare it to the basic approach from Section 3.1, we study a toy example. Consider the curve shaped like a seam line of a tennis ball, given by the parametrization

$$\begin{aligned} x &= a \cos t + b \cos 3t, & y &= a \sin t - b \sin 3t, \\ z &= 2\sqrt{ab} \sin 2t, & \text{with } a &= 0.8, b = 0.2, \end{aligned} \quad (23)$$

and take a cloud of 100 points generated by adding normally distributed noise to random points on the curve. The curve,

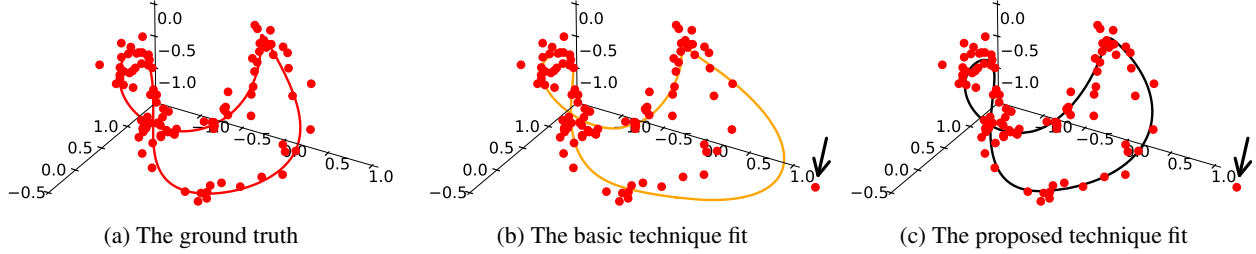


Figure 2: The point cloud of 99 points is generated by adding Gaussian noise to random points lying on the ground truth curve. A random outlier (under the arrow) having twice the norm of the points on the curve is then added to the point cloud. The ground truth, the fit of the basic technique from Section 3.1 and of the proposed technique from Section 3.4 are shown.

point cloud and results of application of both the basic algorithm and the proposed technique are illustrated on Figure 2. We can see that the changes suggested in Sections 3.2 and 3.3 succeed at making the technique more robust.

4.2. Outlier detection in a face recognition problem

We consider an image classification pipeline consisting of a face detection and alignment algorithm (MTCNN, Xiang and Zhu (2017)), deep feature extractor (ArcFace, Deng et al. (2019)) and cosine similarity based classifier. In this setting, we fit a quadric intersection manifold to the 512-dimensional feature space embeddings of the dataset used to train the deep feature extractor. We then measure the performance of the quadric intersection based outlier detector and the performance of the cosine similarity improved by penalizing the outliers detected by it. The quadric based approach is compared to the PCA based baseline that fits a linear subspace to data. We also compare our technique to the baseline approach based on the embedding norm, that is motivated by recent work of Yu et al. (2020) that shows that in the face recognition domain, the norm of an embedding might carry some information on the image outlieriness.

The deep feature extractor was trained on the MS1M dataset (Guo et al., 2016).⁶ The embeddings generated by the trained feature extractor were used to fit the quadric intersection manifold and PCA’s linear subspace. Motivated by a simple ablation study (see details in Appendix B), the number of quadrics was set to 300 and the dimension of the PCA plane was set to 170. Fitting an intersection of 300 quadrics took us 72 hours on a pair of Quadro RTX 8000 GPUs, using an unoptimized implementation. The resulting quadric intersection model occupies around 150MB.

⁶We used the MS1M-ArcFace modification of the dataset from <https://github.com/deepinsight/insightface/wiki/Dataset-Zoo> and the Anime-Faces dataset from <https://github.com/bchao1/Anime-Face-Dataset>.

Outlier detection We construct a contaminated dataset by mixing the in-distribution photos from one of the special face recognition datasets with the out-of-distribution photos in the approximate ratio of 99 to 1. The out-of-distribution photos contain 235 manually picked photos from the CPLFW dataset (Zheng and Deng, 2018) where a face cannot be uniquely recognized by a human (e.g. photos of people in hockey helmets, photos with multiple faces) and 235 images from the Anime-Faces dataset⁶ aligned by the MTCNN.

We evaluate the performance of the quadric-based outlier detector based on the score defined in (20). We compare to an outlier detector based on the distance from a point to its projection onto the linear subspace found by PCA, and to an outlier detector based on the embedding Euclidean norm (here, lower norm corresponds to a higher outlier score). The AUC-ROC values for different detectors are presented in the Table 1. A set of representative outliers found by each of the three detectors inside the contaminated (sample of) VGGFace2 dataset is presented in Figure 3.

Dataset	Quadrics	PCA	Norms
MS1M (train)	0.97 (10^{-4})	0.89 (10^{-4})	0.75 (10^{-4})
MegaFace (a)	0.89 (10^{-4})	0.81 (10^{-3})	0.74 (10^{-4})
VGGFace2 (b)	0.96 (10^{-4})	0.88 (10^{-4})	0.75 (10^{-4})
FFHQ (c)	0.92 (10^{-4})	0.90 (10^{-4})	0.72 (10^{-3})
CPLFW (d)	0.93	0.82	0.75
CALFW (e)	0.97	0.88	0.70

Table 1: The AUC-ROC scores for different feature space outlier detectors. For the larger datasets the order of standard deviation that is estimated from 10 random subsamplings is given in brackets. Here (a), (b), (c), (d), (e) correspond respectively to Kemelmacher-Shlizerman et al. (2016), Cao et al. (2018), Karras et al. (2019), Zheng and Deng (2018), Zheng et al. (2017). (b) has been taken from <https://github.com/deepinsight/insightface/wiki/Dataset-Zoo>.



Figure 3: Manually selected representative outliers from 64 images with the highest outlier score according to quadrics (top row), PCA (middle row) and norms (bottom row) from the first 10^4 images of VGGFace2 dataset. All 64 outliers with highest score are presented in Appendix B.

Similarity metric robustification Here we consider the previously-mentioned Cross-Posed Labeled Faces in the Wild (CPLFW) dataset which is particularly challenging due to the presence of the pictures that cannot be recognized even by a human (which we consider as outliers). We apply three different robustification methods to cosine similarity, and measure their performance in terms of the identification rate (IR). This can be understood as the true positive rate of the similarity-based classifier solving an identification problem in a presence of distractors taken from the MegaFace dataset, see details in Appendix B.

All three robustification methods are based upon the equation (22): the first one is based on the outlier score corresponding to the quadric intersection model, the second one on the PCA-related outlier score, and the third one on the norm-related outlier score (the corresponding outlier scores were reviewed in the discussion on outlier detection above).

Robustification method	IR (full)	IR (no distractors)
No robustification	0.595	0.666
Quadrics	0.636	0.743
PCA	0.626	0.720
Embedding norm	0.636	0.738

Table 2: Effect of the various modifications of similarity on the identification rate. False positive rate is fixed to 10^{-5} .

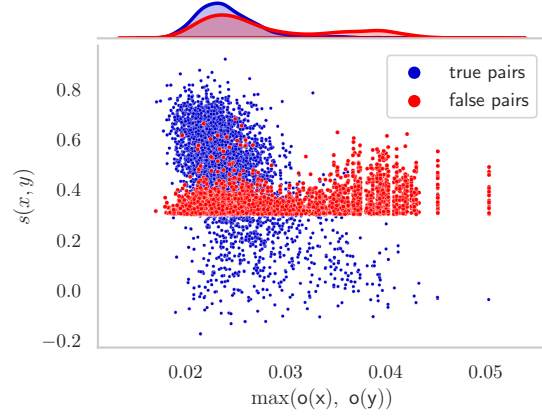


Figure 4: Scatter plot of the $2 \cdot 10^4$ true pairs (same class) and the same number of false pairs (different class) with highest similarity. Top: the distribution of quadric based outlier score for true and false pairs.

The IR corresponding to each of the three robustification methods is presented in Table 2. Both quadrics and norms perform similarly in this experiment, outperforming PCA.

Figure 4 gives some intuition on how does the suggested robustification method work. We can see that a substantial portion of false pairs (different class) which have high cosine similarity can be separated by detecting the high value of the quadric based outlier score.

Discussion Quadric based techniques behave favorably in both the outlier detection and similarity metric robustification problems, improving on the PCA baseline. The norm based baseline turns out to be a stronger competitor, which is not surprising given that it is specialized to the setting at hand. Our approach, which is generic, matches its performance in similarity metric robustification, and improves upon its performance it on outlier detection.

5. Conclusion

We describe a manifold learning technique based on fitting an intersection of quadrics to a point cloud. Building on a particular instance of non-linear PCA, we introduce a number of improvements that promote robustness and equivariance, while reducing the task of fitting an intersection of quadrics to solving a particular optimization problem. This problem is tractable in moderately high dimension, such as the feature space of a deep representation learning model, is amenable to minibatch training, and thus scales well with respect to point cloud size. The learned quadric intersection can be used to define an outlier score and to improve a given similarity metric. We demonstrate and benchmark the proposed approach empirically on an image classification task.

Acknowledgments

FP was supported by the Russian Academic Excellence Project 5-100 within the framework of the Basic Research Program at HSE University. SI and AZ were supported by the Ministry of Science and Higher Education of the Russian Federation, agreement № 075-15-2019-1619. VB was supported by the Ministry of Science and Higher Education of the Russian Federation, agreement № 075-15-2019-1620.

References

- N. Bansal, X. Chen, and Z. Wang. Can we gain more from orthogonality regularizations in training deep networks? *Advances in Neural Information Processing Systems*, 31:4261–4271, 2018. Cited on page 5.
- D. Beale, Y.-L. Yang, N. Campbell, D. Cosker, and P. Hall. Fitting quadrics with a Bayesian prior. *Computational Visual Media*, 2(2):107–117, 2016. Cited on page 3.
- M. Belkin and P. Niyogi. Laplacian eigenmaps and spectral techniques for embedding and clustering. *Advances in neural information processing systems*, 14:585–591, 2001. Cited on page 2.
- E. J. Candès, X. Li, Y. Ma, and J. Wright. Robust principal component analysis? *Journal of the ACM (JACM)*, 58(3):1–37, 2011. Cited on page 4.
- Q. Cao, L. Shen, W. Xie, O. M. Parkhi, and A. Zisserman. Vggface2: A dataset for recognising faces across pose and age. In *2018 13th IEEE International Conference on Automatic Face & Gesture Recognition (FG 2018)*, pages 67–74. IEEE, 2018. Cited on page 7.
- J. Deng, J. Guo, N. Xue, and S. Zafeiriou. Arcface: Additive angular margin loss for deep face recognition. In *Proceedings of the IEEE Conference on Computer Vision and Pattern Recognition*, pages 4690–4699, 2019. Cited on pages 1, 6, 7.
- J. Devlin, M.-W. Chang, K. Lee, and K. Toutanova. Bert: Pre-training of deep bidirectional transformers for language understanding. *arXiv preprint arXiv:1810.04805*, 2018. Cited on page 1.
- B. Du and L. Zhang. A discriminative metric learning based anomaly detection method. *IEEE Transactions on Geoscience and Remote Sensing*, 52(11):6844–6857, 2014. Cited on page 1.
- C. Fefferman, S. Mitter, and H. Narayanan. Testing the manifold hypothesis. *Journal of the American Mathematical Society*, 29(4):983–1049, 2016. Cited on page 2.
- Y. Guo, L. Zhang, Y. Hu, X. He, and J. Gao. MS-Celeb-1M: A Dataset and Benchmark for Large-Scale Face Recognition, 2016. arXiv: 1607.08221 [cs.CV]. Cited on page 7.
- J. Harris. *Algebraic geometry: a first course*, volume 133. Springer Science & Business Media, 2013. Cited on page 3.
- T. Karras, S. Laine, and T. Aila. A style-based generator architecture for generative adversarial networks. In *Proceedings of the IEEE conference on computer vision and pattern recognition*, pages 4401–4410, 2019. Cited on page 7.
- I. Kemelmacher-Shlizerman, S. M. Seitz, D. Miller, and E. Brossard. The megaface benchmark: 1 million faces for recognition at scale. In *Proceedings of the IEEE Conference on Computer Vision and Pattern Recognition*, pages 4873–4882, 2016. Cited on page 7.
- J. A. Lee and M. Verleysen. *Nonlinear dimensionality reduction*. Springer Science & Business Media, 2007. Cited on page 2.
- S. Liao, Z. Lei, D. Yi, and S. Z. Li. A benchmark study of large-scale unconstrained face recognition. In *IEEE international joint conference on biometrics*, pages 1–8. IEEE, 2014. Cited on page 13.
- D. Lunga, S. Prasad, M. M. Crawford, and O. Ersoy. Manifold-learning-based feature extraction for classification of hyperspectral data: A review of advances in manifold learning. *IEEE Signal Processing Magazine*, 31(1):55–66, 2013. Cited on page 1.
- Y. Ma and Y. Fu. *Manifold learning theory and applications*. CRC press, 2011. Cited on page 2.
- L. v. d. Maaten and G. Hinton. Visualizing data using t-SNE. *Journal of machine learning research*, 9(Nov):2579–2605, 2008. Cited on page 2.
- L. McInnes, J. Healy, N. Saul, and L. Großberger. UMAP: Uniform Manifold Approximation and Projection. *Journal of Open Source Software*, 3(29):861, 2018. Cited on page 2.
- J. Milnor and D. W. Weaver. *Topology from the differentiable viewpoint*. Princeton university press, 1997. Cited on page 2.
- D. Mumford. Varieties defined by quadratic equations. In *Questions on algebraic varieties*, pages 29–100. Springer, 2010. Cited on page 1.

- N. Patwari, A. O. Hero III, and A. Pacholski. Manifold learning visualization of network traffic data. In *Proceedings of the 2005 ACM SIGCOMM workshop on Mining network data*, pages 191–196, 2005. Cited on page 1.
- S. T. Roweis and L. K. Saul. Nonlinear dimensionality reduction by locally linear embedding. *science*, 290(5500):2323–2326, 2000. Cited on page 2.
- B. Schölkopf, A. Smola, and K.-R. Müller. Nonlinear component analysis as a kernel eigenvalue problem. *Neural computation*, 10(5):1299–1319, 1998. Cited on page 2.
- G. Taubin. An improved algorithm for algebraic curve and surface fitting. In *1993 (4th) International Conference on Computer Vision*, pages 658–665. IEEE, 1993. Cited on pages 3, 4, 12.
- G. Taubin. Estimation of planar curves, surfaces, and non-planar space curves defined by implicit equations with applications to edge and range image segmentation. *IEEE Transactions on Pattern Analysis & Machine Intelligence*, (11):1115–1138, 1991. Cited on pages 3, 5.
- J. B. Tenenbaum, V. De Silva, and J. C. Langford. A global geometric framework for nonlinear dimensionality reduction. *science*, 290(5500):2319–2323, 2000. Cited on page 2.
- R. Vidal, Y. Ma, and S. Sastry. Generalized principal component analysis (GPCA). *IEEE transactions on pattern analysis and machine intelligence*, 27(12):1945–1959, 2005. Cited on page 4.
- J. Xiang and G. Zhu. Joint face detection and facial expression recognition with MTCNN. In *2017 4th International Conference on Information Science and Control Engineering (ICISCE)*, pages 424–427. IEEE, 2017. Cited on page 7.
- C. Yu, X. Zhu, Z. Lei, and S. Z. Li. Out-of-Distribution Detection for Reliable Face Recognition. *IEEE Signal Processing Letters*, 27:710–714, 2020. Cited on page 7.
- T. Zheng and W. Deng. Cross-pose lfw: A database for studying cross-pose face recognition in unconstrained environments. *Beijing University of Posts and Telecommunications, Tech. Rep*, 5, 2018. Cited on page 7.
- T. Zheng, W. Deng, and J. Hu. Cross-age lfw: A database for studying cross-age face recognition in unconstrained environments. *arXiv preprint arXiv:1708.08197*, 2017. Cited on page 7.

A. Theory

A.1. Additional details on the connection to PCA

Let f_1, \dots, f_m be quadratic polynomials in \mathbb{R}^d and $v(f_1), \dots, v(f_m) \in \mathbb{R}^D$ be their coefficient vectors (see Section 3.1) that we assume to be orthonormal. We denote by $\mathcal{V}_m \subseteq \mathbb{R}^D$ the vector space spanned by these vectors and by \mathcal{V}_m^\perp its orthogonal completion. For each $u \in \mathbb{R}^D$ we denote by $\text{pr}(u)$ its orthogonal projection onto \mathcal{V}_m . It is defined by the formula

$$\text{pr}(u) = \sum_{k=1}^m \langle u, v(f_k) \rangle \cdot v(f_k). \quad (24)$$

Therefore the following holds for the distance $d(u, \mathcal{V}_m^\perp)$ from u to \mathcal{V}_m^\perp :

$$d(u, \mathcal{V}_m^\perp)^2 = \|\text{pr}(u)\|^2 = \sum_{k=1}^m \langle u, v(f_k) \rangle^2. \quad (25)$$

Let $\varphi : \mathbb{R}^d \rightarrow \mathbb{R}^D$ be the feature map (8). Then for a quadratic polynomial f we have, for all $p \in \mathbb{R}^d$,

$$f(p) = \langle \varphi(p), v(f) \rangle. \quad (26)$$

Using the formulas (25) and (26) we obtain

$$\sum_{j=1}^n \sum_{k=1}^m |f_k(p_j)|^2 = \sum_{j=1}^n \sum_{k=1}^m \langle \varphi(p_j), v(f_k) \rangle^2 = \sum_{j=1}^n \|\text{pr}(\varphi(p_j))\|^2 = \sum_{j=1}^n d(\varphi(p_j), \mathcal{V}_m^\perp)^2, \quad (27)$$

which proves equation (9).

It follows that the optimization problem (7) is equivalent to minimization of $\sum_{j=1}^n d(\varphi(p_j), \mathcal{V}_m^\perp)^2$, which is similar to the optimisation problem that PCA solves. Note that here we do not assume that the point cloud $\varphi(p_1), \dots, \varphi(p_n)$ is centered, so the optimization problem (7) is equivalent to the non-centered version of PCA.

A.2. Non-equivariance of the optimization problem (7)

On the pictures below we show an example of two point clouds on the plane and the corresponding quadrics that solve the optimization problem (7) exactly. The point cloud on Figure 5 (b) can be obtained by shifting the point cloud on Figure 5 (a) by vector $(10, 0)$. However, the corresponding quadrics are not the shifts of each other.

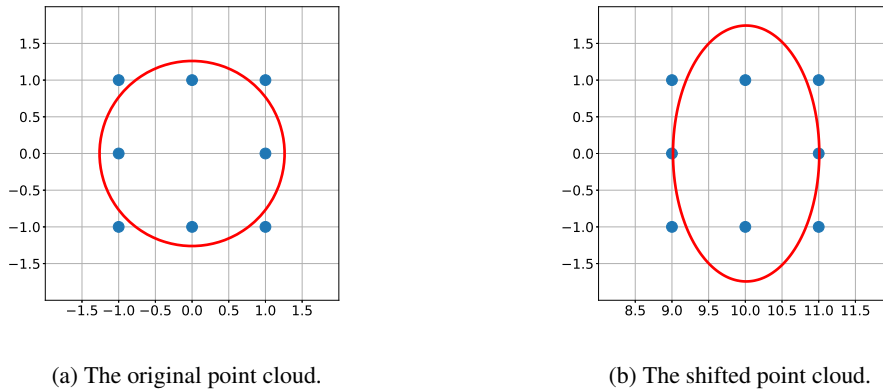


Figure 5: A point cloud and its shifted version (blue) and the respective quadrics (red) that solve the optimization problem (7).

A.3. Approximation distance of order k

Let $f : \mathbb{R}^d \rightarrow \mathbb{R}$ be a polynomial. For a multi-index $I = (i_1, \dots, i_d)$ we denote by C_I the coefficient of the Taylor polynomial of f in the point p corresponding to the monomial $x_1^{i_1} \dots x_d^{i_d}$:

$$C_I = \frac{1}{I!} \frac{\partial^{|I|} f}{\partial x_1^{i_1} \dots \partial x_d^{i_d}}(p), \quad (28)$$

where $|I| = i_1 + \dots + i_d$ and $I! = i_1! i_2! \dots i_d!$.

For each integer $l \geq 1$ we set

$$c_l = - \left(\sum_{|I|=l} C_I^2 / b(I) \right)^{1/2}, \quad (29)$$

where $b(I) = |I|! / I!$ is the multinomial coefficient and $c_0 = |f(p)|$. Note that $c_0 \geq 0$ and $c_l \leq 0$ for $l \geq 1$. With this, the polynomial $\sum_{l=0}^k c_l t^l$ has a unique non-negative root. We denote this root by $d_k(p, Z(f))$ and, following Taubin (1993), call it *the approximation distance of order k* . Note that $d_k(p, Z(f))$ depends on p and f , not only on p and the zero set $Z(f)$, despite the notation.

If $f(x) = x^\top A x + b x + c$ is a quadratic polynomial, then it is easy to check that $c_2 = \|A\|_{HS}$. Using this and the formula for the roots of the general quadratic equation we obtain the formula

$$d_2(p, Z(f)) = \frac{\sqrt{h^2 + |f(p)| \|f\|_{HS}} - h}{\|f\|_{HS}}, \quad (30)$$

where $h = \|\nabla f(p)\|/2$. In particular, if $\|f\|_{HS} = 1$, we have a particularly simple expression

$$d_2(p, Z(f)) = \sqrt{h^2 + |f(p)|} - h. \quad (31)$$

A.4. Equivariance of the approximation distance order k

The coefficients of the polynomial $c_0 + c_1 t + \dots + c_k t^k$ from the definition of $d_k(p, Z(f))$ depend only on the coefficients of the Taylor polynomial of degree k of the map f at point p . We denote this polynomial by $T_{k,f,p}$. In order to prove the equivariance of the k -distance, i.e. $d_k(\theta(p), Z(f \circ \theta)) = d_k(p, Z(f))$, it is enough to show the equivariance of the Taylor polynomial, in the sense that

$$T_{k,p,f} \circ \theta = T_{k,f \circ \theta, \theta(p)}. \quad (32)$$

The defining property of the Taylor polynomial is the following: $T_{k,f,p}$ is the only polynomial of degree $\leq k$ such that

$$\|T_{k,f,p}(x) - f(x)\| = o(\|x - p\|^k) \quad \text{as } x \rightarrow p. \quad (33)$$

Any isometry $\theta : \mathbb{R}^d \rightarrow \mathbb{R}^d$ is of form $\theta(x) = Q \cdot x + v$, where Q is an orthogonal matrix and v is some vector. Hence $T_{k,f,p} \circ \theta$ is also a polynomial of degree $\leq k$. The equation (33) then implies

$$\|(T_{k,f,p} \circ \theta)(x) - (f \circ \theta)(x)\| = o(\|\theta(x) - \theta(p)\|^k) = o(\|x - p\|^k) \quad \text{as } x \rightarrow p. \quad (34)$$

Therefore $T_{k,p,f} \circ \theta = T_{k,f \circ \theta, \theta(p)}$.

A.5. Equivariance of the Hilbert-Schmidt inner product

The Hilbert-Schmidt inner product of matrices can be written as

$$\langle A, B \rangle_{HS} = \text{tr}(A^\top \cdot B) = \text{tr}(B^\top \cdot A), \quad (35)$$

where $\text{tr}(\cdot)$ denotes the trace of a matrix. It follows that for any orthogonal matrix Q the following holds

$$\langle A, B \rangle_{HS} = \langle AQ, BQ \rangle_{HS} = \langle QA, QB \rangle_{HS}. \quad (36)$$

Recall that any isometry $\theta : \mathbb{R}^d \rightarrow \mathbb{R}^d$ is of form $\theta(x) = Q \cdot x + v$, where Q is an orthogonal matrix and v is a vector. If f is a quadratic polynomial with the corresponding matrix A (in the sense of equation (13)), then $f \circ \theta$ is a quadratic polynomial whose corresponding matrix equals to $Q^\top A Q$. Therefore the equation (36) implies

$$\langle f \circ \theta, g \circ \theta \rangle_{HS} = \langle Q^\top A Q, Q^\top B Q \rangle_{HS} = \langle A, B \rangle_{HS} = \langle f, g \rangle_{HS}. \quad (37)$$

B. Additional experimental details

B.1. Datasets construction

The embeddings for the used datasets are constructed by the pretrained ArcFace model LResNet100E-IR, ArcFace@ms1m-refine-v2⁷. For MegaFace, FFHQ, CALFW and CPLFW datasets additional alignment is done by MTCNN. For CPLFW, due to the complex nature of the dataset, the photos where MTCNN failed to detect a face were preserved in the dataset, with no additional preprocessing applied apart from resizing. Aligned versions of MS1M-ArcFace and VGGFace2 datasets are taken from <https://github.com/deepinsight/insightface/wiki/Dataset-Zoo>.

B.2. Ablation study

The results of the simple ablation study used to identify the best number of quadrics in intersection and the optimal number of principal components in the setting of Section 4.2 are presented here. AUC-ROC and IR scores are given in Table 3 and Table 4 respectively. The preliminary selection of numbers of principal components were made by studying the eigenvalue decay. Although in our tests the quadric based methods’ performance is almost independent on the number of quadrics in the intersection, we pick 300 to better match the dimension of the 170-dimensional PCA plane that shows best performance.⁸

Dataset	Quadrics				PCA		
	100 quadrics	200 quadrics	300 quadrics	400 quadrics	130-dim	170-dim	200-dim
MS1M (train)	0.97(10 ⁻⁴)	0.97(10 ⁻⁴)	0.97(10 ⁻⁴)	0.98(10 ⁻⁴)	0.88 (10 ⁻⁴)	0.89 (10 ⁻⁴)	0.87 (10 ⁻³)
MegaFace	0.89(10 ⁻³)	0.89(10 ⁻³)	0.89(10 ⁻³)	0.89(10 ⁻³)	0.79 (10 ⁻³)	0.81 (10 ⁻³)	0.81 (10 ⁻³)
VGGFace2	0.96(10 ⁻⁴)	0.96(10 ⁻⁴)	0.96(10 ⁻⁴)	0.96(10 ⁻⁴)	0.86 (10 ⁻³)	0.88 (10 ⁻⁴)	0.86 (10 ⁻³)
FFHQ	0.93(10 ⁻⁴)	0.93(10 ⁻⁴)	0.92(10 ⁻⁴)	0.93(10 ⁻⁴)	0.89 (10 ⁻³)	0.90 (10 ⁻⁴)	0.89 (10 ⁻³)
CPLFW	0.93	0.93	0.93	0.93	0.80	0.82	0.80
CALFW	0.98	0.97	0.97	0.98	0.88	0.88	0.85

Table 3: AUC-ROC scores depending on the number of quadrics in the intersection for the quadrics based outlier detector and AUC-ROC scores depending on the number of principal components for the PCA based outlier detector.

Metric	Quadrics				PCA		
	100 quadrics	200 quadrics	300 quadrics	400 quadrics	130-dim	170-dim	200-dim
IR (full)	0.635	0.635	0.636	0.637	0.620	0.626	0.710
IR (no distractors)	0.741	0.742	0.743	0.746	0.611	0.720	0.700

Table 4: IR score for the face identification problem with quadric-based and PCA-based robustification depending (respectively) on the number of quadrics in the intersection or on the number of principal components.

B.3. Identification rate

Here we describe the procedure for evaluating the performance of the similarity function s on the identification problem on the set X of face images with the additional set Y of distractor images. It is based on the metric called *identification rate* and is widely used in the face recognition domain (Liao et al., 2014).

First, define a family of classifiers C_a , parametrized by $a \in \mathbb{R}$ as follows: C_a declares a pair $p = (x, y)$ positive (same class), if $s(x, y) \geq a$. The corresponding false positive rate and true positive rate are denoted by $\text{fpr}(a)$ and $\text{tpr}(a)$ respectively. For a fixed false positive rate $f \in [0, 1]$ we define the similarity threshold $\text{sth}(f)$ by

$$\text{sth}(f) = \sup\{a \in \mathbb{R} \mid \text{fpr}(a) \leq f\}. \quad (38)$$

The *identification rate (without distractors)* is defined to be $\text{tpr}(\text{sth}(f))$.

⁷<https://github.com/deepinsight/insightface/wiki/Model-Zoo>

⁸Recall that, at least in the non-degenerate case, the dimension of the intersection of k quadrics in d -dimensional space is $d - k$.

Consider the set

$$Q = \{(x, y) \in X \times X \mid \forall d \in Y \ s(x, y) > \max(s(x, d), s(y, d))\}, \quad (39)$$

which contains pairs *that cannot be distracted* by elements of Y and consider the binary classifier that declares a pair (x, y) positive (same class) if it is positive with respect to the classifier $C_{\text{sth}(f)}$ and it cannot be distracted. The corresponding tpr is called the *identification rate (full)*.

In our experiments the subset of first $8 \cdot 10^5$ embeddings of the MegaFace dataset is used as the distractor set Y .

B.4. Similarity metric robustification hyperparameters

The threshold hyperparameters (chosen by grid search) for various robustification methods (as in (22)) are as follows:

- Quadrics, $t = 0.034$,
- PCA, $t = 0.535$,
- Norms, $t = 18$.

B.5. Outlier photos

For each of the three outlier detectors (quadric-based, PCA-based, norm-based) we show here the set of 64 images with highest outlier score from the first 10^4 images of VGGFace2 dataset. Images are sorted in descending order of scores. The images corresponding to the quadric-based, PCA-based and norm-based outlier detectors are shown in Figure 6, Figure 7 and Figure 8 respectively.

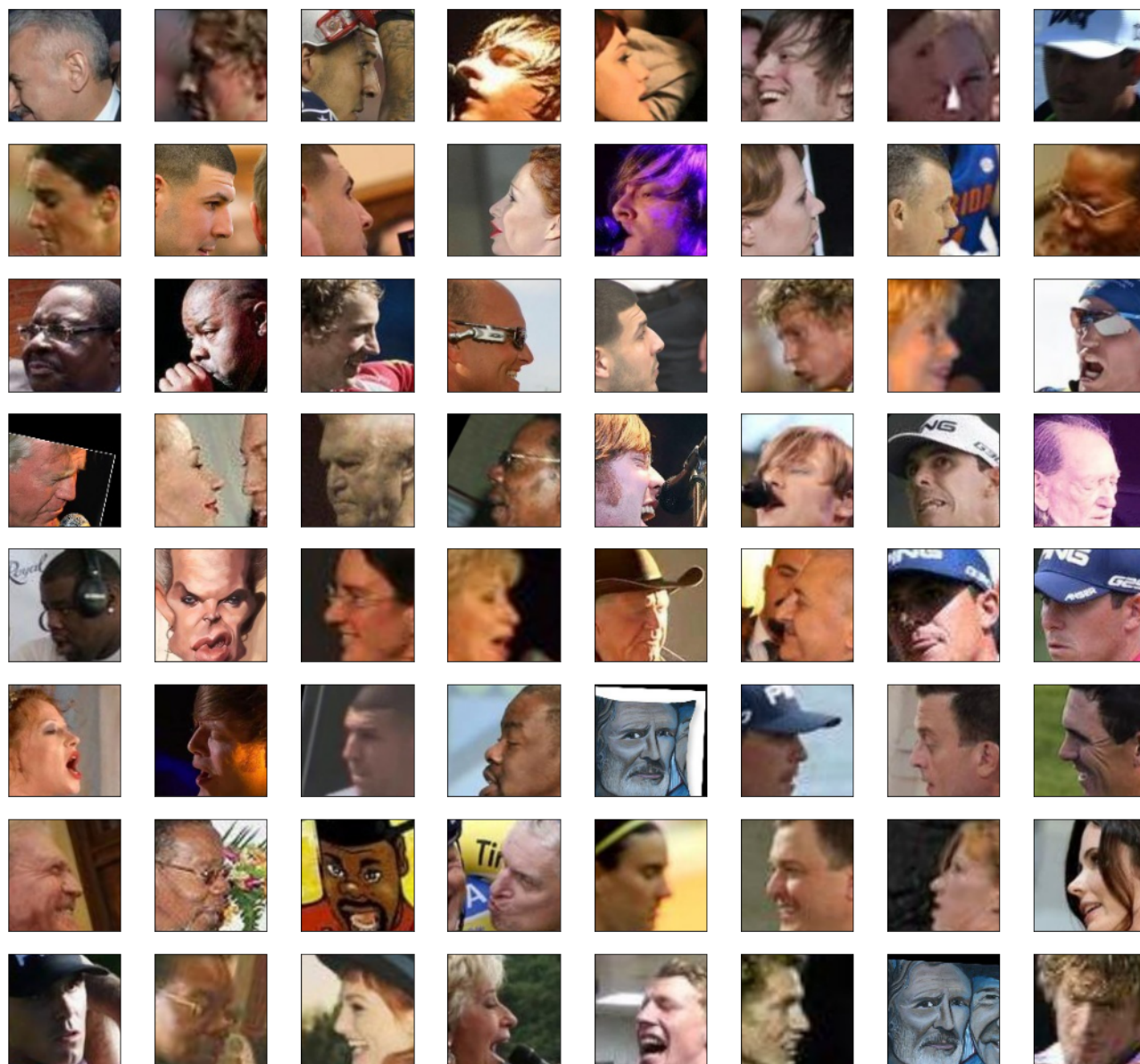


Figure 6: Highest outlier score images detected by quadrics

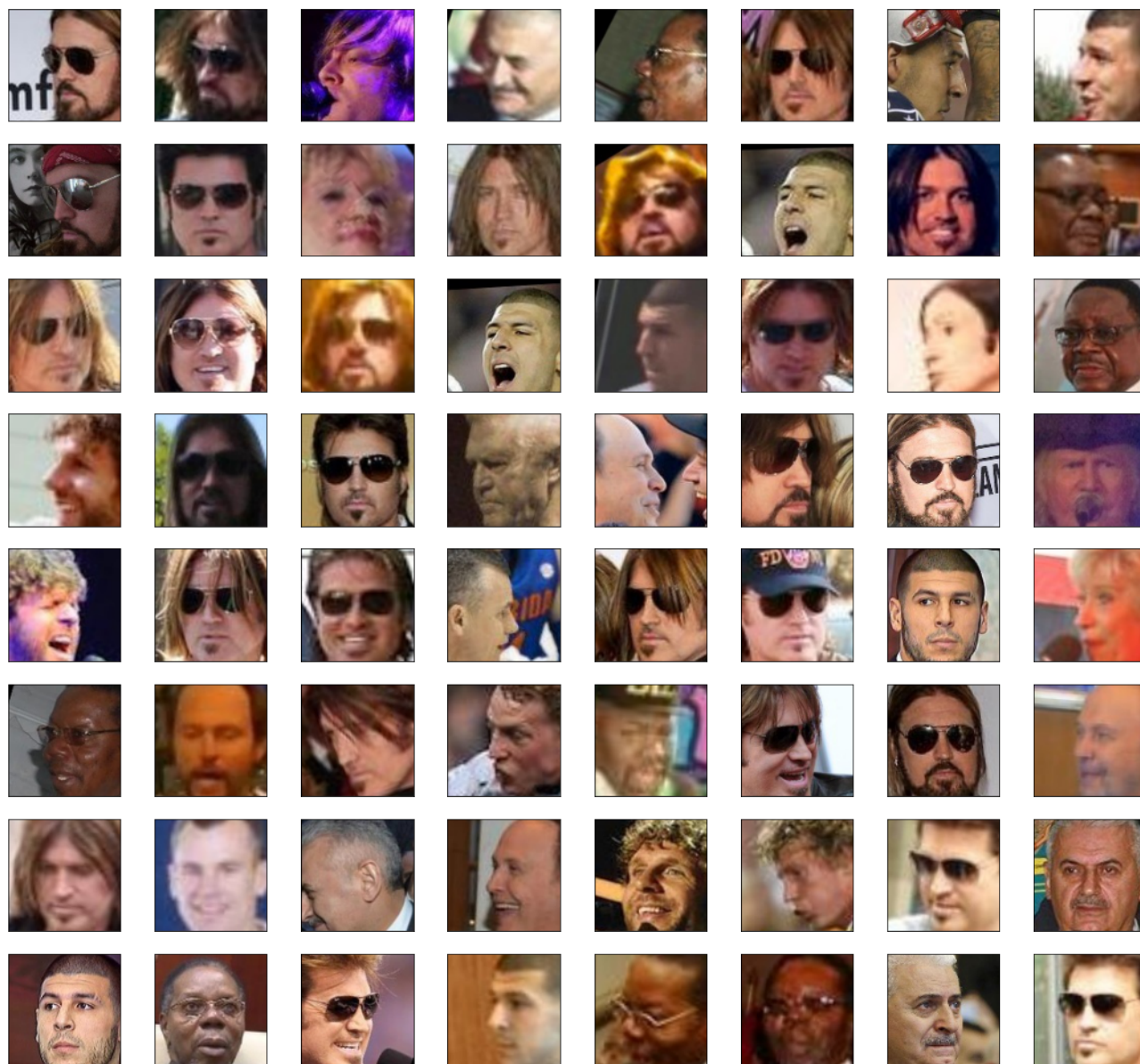


Figure 7: Highest outlier score images detected by PCA

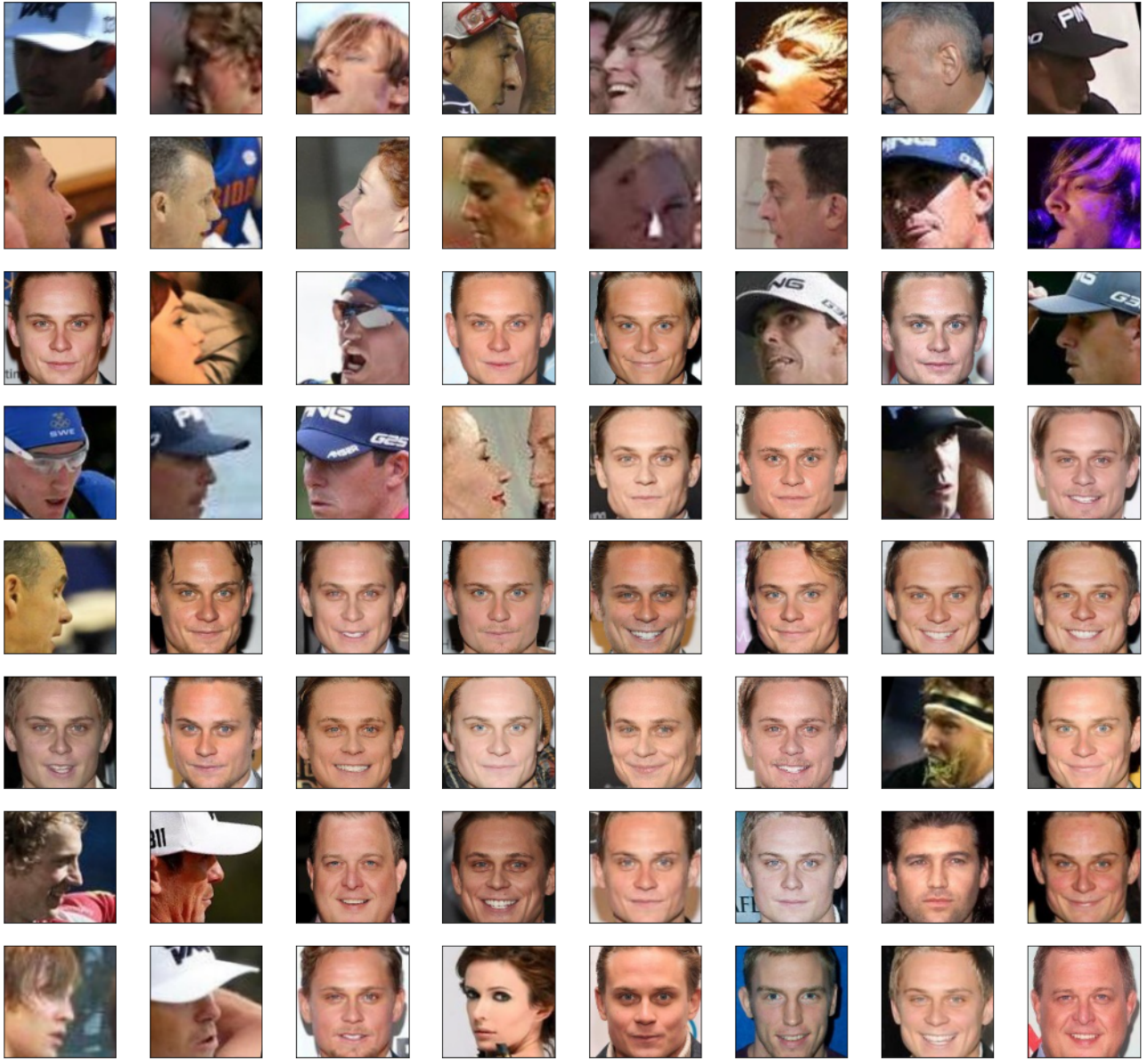


Figure 8: Highest outlier score images detected by norms